Brazilian Journal
of Chemical
Engineering

ISSN 0104-6632
Printed in Brazil
www.abeq.org.br/bjche

Vol. 32, No. 02, pp. 609 - 627, April - June, 2015
dx.doi.org/10.1590/0104-6632.20150322s00003417

# APPLICATION OF A SURFACE-RENEWAL MODEL TO PERMEATE-FLUX DATA FOR CONSTANT-PRESSURE CROSS-FLOW MICROFILTRATION WITH DEAN VORTICES

G. Idan and S. G. Chatterjee*

Department of Paper and Bioprocess Engineering, SUNY College of Environmental Science and Forestry, 1 Forestry Drive, Syracuse, New York 13210, USA.
Phone: +1-315-470-6517, Fax: +1-315-470-6945
E-mail: schatterjee@esf.edu

*(Submitted: April 5, 2014 ; Revised: September 22, 2014 ; Accepted: October 14, 2014)*

**Abstract** - The introduction of flow instabilities into a microfiltration process can dramatically change several elements such as the surface-renewal rate, permeate flux, specific cake resistance, and cake buildup on the membrane in a positive way. A recently developed surface-renewal model for constant-pressure, cross-flow microfiltration (Hasan *et al*., 2013) is applied to the permeate-flux data reported by Mallubhotla and Belfort (1997), one set of which included flow instabilities (Dean vortices) while the other set did not. The surface-renewal model has two forms ─ the complete model and an approximate model. For the complete model, the introduction of vortices leads to a 53% increase in the surface- renewal rate, which increases the limiting (i.e., steady-state) permeate flux by 30%, decreases the specific cake resistance by 14.5% and decreases the limiting cake mass by 15.5% compared to operation without vortices. For the approximate model, a 50% increase in the value of surface renewal rate is shown due to vortices, which increases the limiting permeate flux by 30%, decreases the specific cake resistance by 10.5% and decreases the limiting cake mass by 13.7%. The cake-filtration version of the critical-flux model of microfiltration (Field *et al*., 1995) is also compared against the experimental permeate-flux data of Mallubhotla and Belfort (1997). Although this model can represent the data, the quality of its fit is inferior compared to that of the surface-renewal model.
*Keywords*: Critical-flux model; Dean vortices; Microfiltration; Surface-renewal model.

## INTRODUCTION

Microfiltration is the physical removal of solid particles from a liquid by means of a membrane in order to concentrate suspensions. It is similar to ultrafiltration and nanofiltration with the difference being the pore size of the membrane (Cheryan, 1998). This technique is often used to separate cells, proteins and bacteria from a liquid (e.g., fermentation broths) and in wastewater treatment, besides having numerous biotech uses like enzyme recovery (Kroner *et al.*, 1984; Le *et al.*, 1984; Marston *et al.*, 1984), hormone production (Shoner *et al.*, 1985), protein recovery (Titchener-Hooker *et al.*, 1991), and cell lysate recovery (Bailey and Meagher, 1997a, 1997b). In cross-flow membrane filtration, an incoming feed solution or suspension flows across the surface of a membrane and the permeate flow is that portion of the liquid which passes through the membrane in a direction perpendicular to that of the main flow.

Figures 1 and 2 show two common process flow diagrams of cross-flow microfiltration (CFMF). In

*To whom correspondence should be addressed

Figure 1, both permeate and retentate (i.e., concentrate) are returned to the feed vessel, which is a common practice in laboratory studies; thus, the feed concentration remains invariant with process time. The system shown in Figure 2, in which only the retentate is returned to the feed vessel, is used in industry to concentrate a feed suspension (Rudolph and MacDonald, 1994); here the feed concentration changes with process time. The analysis presented in this paper is concerned with the system shown in Figure 1. Depending upon the application, the filtration membrane can be either polymeric or ceramic and contained in a module which comes in different configurations, e.g., tubular, spiral wound and hollow fiber.

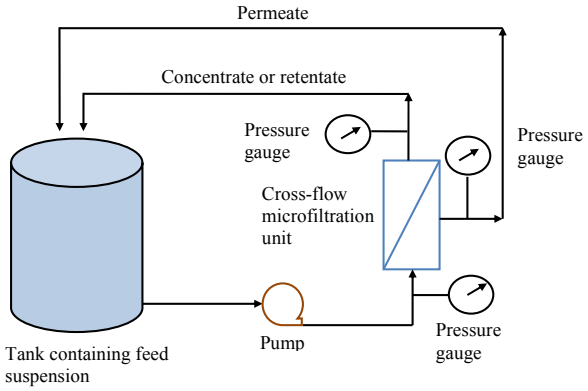


**Figure 1:** Schematic representation of a laboratory-scale microfiltration unit with both permeate and concentrate returned to the feed tank.

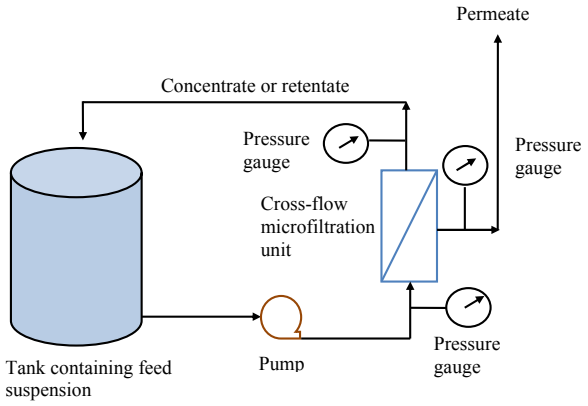


**Figure 2:** Schematic representation of an industrial-scale microfiltration unit with only the concentrate returned to the feed tank (adapted from Rudolph and MacDonald, 1994).

There is a common problem with any filtration process whether it is microfiltration, ultrafiltration, vacuum filtration, or gravity-driven filtration (typical in student laboratories). This problem is the decline of the permeate flux with process time. The importance of understanding the permeate-flux decline is crucial for industrial processes, laboratory practices or other uses of filtration since it is important to maintain a high permeate flow rate so that the process can be run in a reasonable amount of time, which translates into the efficiency and cost of the whole operation. The decline of permeate flux looks similar to an exponential-type decay that approaches a zero value for dead-end filtration, but a final nonzero value in the case of cross-flow filtration. According to Gurian (2010), large-scale microfiltration has not been competitive cost-wise in the past, but is now being adopted in plants with design flows as large as 20 MGD (million gallons per day). The modeling of CFMF can contribute to the effectiveness and efficiency of membrane technologies, including the scale-up of such technologies from the laboratory- or pilot-scale to the industrial scale.

It is commonly held that the primary reasons for permeate-flux decline are two fouling mechanisms known as pore blocking and cake formation. As soon as the CFMF operation is started, some of the particles in the feed suspension become lodged in the pores of the filter, which can be blocked either partially or completely. This phenomenon, according to Song (1998), is a rapid process with barely one layer of particles sufficing to complete maximum blocking of the membrane, and is the cause of permeate flux decline during the initial moments of filtration. As time goes on, solid or colloidal particles begin to collide, forming, at first, a few layers on the membrane wall — a phenomenon called "gel polarization." With the further progress of time, these layers build upon one another and form a "cake" on the membrane surface. In this phase, the cake resistance increases as the cake gets thicker and flux decline continues until the cake layer attains an equilibrium thickness, when a steady-state (nonzero) plateau in the permeate flux is established.

In a series of publications, Belfort and co-workers conducted comprehensive theoretical and experimental investigations on the nature of the flow field in curved channels and the effects of the resulting centrifugal instabilities, known as Dean vortices, on the performance of nanofiltration, ultrafiltration and microfiltration membrane modules (Chung *et al*., 1996; Mallubhotla and Belfort, 1997; Chung *et al*., 1998; Gehlert *et al*., 1998; Mallubhotla *et al*., 1998; Luque *et al*., 1999; Mallubhotla *et al*., 1999; Mallubhotla *et al*., 2001). The central conclusion that can be drawn from this body of work is that such vortices induce back migration of accumulated solute molecules or

particulates away from the membrane wall and dramatically enhance permeation rates compared to operation without vortices, although at the expense of a larger axial pressure drop. Flux improvements of up to 43% have been reported by Mallubhotla and Belfort (1997) in CFMF of particulate suspensions, while Gehlert *et al*. (1998) found enhancements of 30−120% for ultrafiltration and microfiltration of relatively low concentrated baker's yeast suspensions and 30-90% for microfiltration of relatively concentrated beer yeast. The flux enhancement was found to increase with feed flow rate and transmembrane pressure drop, and decrease with increasing feed concentration of suspended matter (Mallubhotla and Belfort, 1997). Although these researchers presented a considerable body of numerical results and experimental data, they did not correlate their data on permeate flux with a coherent theoretical model that could rationally indicate the influence of variables like feed concentration, transmembrane pressure drop, axial velocity, etc. on the behavior of the permeate flux with process time.

The surface-renewal concept has been used to theoretically model cross-flow microfiltration and ultrafiltration by a number of workers (Koltuniewicz, 1992; Koltuniewicz and Noworyta, 1994; Koltuniewicz and Noworyta, 1995; Constenla and Lozano, 1996; Arnot *et al*., 2000; Chatterjee, 2010; Sarkar *et al.*, 2011; Hasan *et al*., 2013, Zhang and Chatterjee, 2014). In contrast to the film and boundary-layer models of cross-flow membrane filtration, the surface-renewal model has the potential to more realistically describe the transfer of dissolved/suspended solids due to Dean vortices mentioned above, and also due to random hydrodynamic impulses generated at the membrane-liquid interface, e.g., due to membrane roughness or by the use of spacers or turbulence promoters.

The surface-renewal model of CFMF (Hasan *et al*., 2013) postulates that the dominant fouling mechanism that causes permeate-flux decline is cake formation, with pore blocking (if any) occurring only during the initial moments of filtration. The three parameters of the model are: $R_m$ (membrane resistance), $k_c$ [a parameter that is related to the specific cake resistance $\alpha$ — see Eq. (7)] and $S$ (rate of renewal of liquid elements at the membrane surface). The values of these parameters were estimated by fitting the model to experimental permeate flow rate data in the CFMF of fermentation broths in laboratory- and pilot-scale units (Hasan *et al*., 2013). The parameter $S$ increases with velocity of the main flow (Koltuniewicz, 1992; Koltuniewicz and Noworyta, 1994; Koltuniewicz and Noworyta, 1995), and can be thought of as a "scouring" term that represents the removal of deposited material from the membrane wall (Arnot *et al*., 2000), and which depends on the level of flow instability. From dimensional considerations, Hasan *et al*. (2013) proposed a correlation for $S$ as a function of the diameter of the membrane channel, axial flow velocity, relative roughness of the membrane wall, and viscosity and density of the feed suspension.

The primary objective of this paper is to investigate whether the surface-renewal model of Hasan *et al*. (2013) can quantitatively explain the permeate-flux data of Mallubhotla and Belfort (1997), which were taken without and with Dean vortices, and to draw appropriate conclusions. A secondary objective is to compare the well-known critical-flux model of microfiltration (Field *et al*., 1995) against the above-mentioned permeate-flux data.

## SURFACE-RENEWAL MODEL

In the surface-renewal model of Hasan *et al*. (2013), it is postulated that the chief fouling mechanism causing permeate-flux decline is cake formation. Flow instabilities are assumed to constantly bring fresh liquid elements from the bulk liquid to the membrane-liquid interface. A liquid element remains at the membrane surface for a certain amount of time, after which it departs and re-mixes with the bulk liquid. Above the surface elements, the liquid is assumed to be well mixed and the concentration of solids constant due to a high rate of transport (because of flow instability) from this location to the bulk liquid. Gradually, a cake layer builds up on the membrane wall, causing a decline in permeate flux with process time until it reaches a steady value. Using the above concept of surface renewal, combining it with classical cake-filtration theory (McCabe *et al*., 1993) and using the (unsteady) Danckwerts distribution function (Danckwerts, 1951) to represent the ages of surface elements, Hasan *et al*. (2013) derived explicit expressions for the permeate flux and cake mass as functions of process time for CFMF; the reader is directed to their paper for details.

For later use, we define the following dimensionless quantities and also give the definition of the extended Euler gamma function $\Gamma(x, y)$:

$$S^* = \frac{S}{2k_c J_0^2} \tag{1}$$

$$t_p^* = St_p \tag{2}$$

$$J_a^*\left(t_p^*\right)=\frac{J_a\left(t_p\right)}{J_0} \tag{3}$$

$$m_{c,a}^*\left(t_p^*\right)=\frac{m_{c,a}\left(t_p\right)J_0k_c}{c_b} \tag{4}$$

$$\Gamma\left(x,y\right)=\int_y^\infty \lambda^{x-1}e^{-\lambda}d\lambda \tag{5}$$

where

$$J_0=\frac{\Delta p}{\mu R_m} \tag{6}$$

and

$$k_c=\frac{\mu c_b\alpha}{\Delta p} \tag{7}$$

In the above, $S$ (assumed to be constant) = the rate of renewal of liquid elements at the membrane surface, $t_p$ = process time, $J_0$ = permeate flux when $t_p = 0$ (assumed equal to the pure water flux in this work; this aspect will be discussed later), $\Delta p$ = trans-membrane pressure drop, $\mu$ = viscosity of the filtrate, $R_m$ = resistance of the membrane or filter medium, $c_b$ = mass of solids deposited in the filter per unit volume of filtrate (approximately equal to the feed concentration), and $\alpha$ = specific cake resistance. Also, $J_a(t_p)$ represents the age-averaged permeate flux, while $m_{c,a}(t_p)$ is the age-averaged mass of cake accumulated per unit area of the membrane surface at process time $t_p$.

In the following, we present the main theoretical results of Hasan *et al*. (2013), which will be designated as the complete model, and also an approximate model, which can be derived from the complete model.

## Complete Model

The dimensionless permeate flux $J_a^*\left(t_p^*\right)$ and cake mass $m_{c,a}^*\left(t_p^*\right)$ are given by the following theoretical expressions (Hasan *et al*., 2013):

$$J_a^*\left(t_p^*\right)=\frac{e^{S^*}}{1-e^{-t_p^*}}\sqrt{\pi S^*}\left[\operatorname{erf}\left(\sqrt{S^*+t_p^*}\right)-\operatorname{erf}\left(\sqrt{S^*}\right)\right] \tag{8}$$

and

$$m_{c,a}^*\left(t_p^*\right)=\frac{e^{S^*}}{\left(1-e^{-t_p^*}\right)\sqrt{S^*}}\left[\Gamma\left(3/2,S^*\right)-\Gamma\left(3/2,S^*+t_p^*\right)\right]-1 \tag{9}$$

It may be shown that as $t_p^* \to 0$:

$$J_a^*\left(t_p^*\to 0\right)=1 \tag{10}$$

and

$$m_{c,a}^*\left(t_p^*\to 0\right)=0 \tag{11}$$

while as $t_p^* \to \infty$:

$$J_a^*\left(t_p^*\to\infty\right)=\frac{J_a\left(t_p\to\infty\right)}{J_0}=\frac{J_{lim}}{J_0}=J_{lim}^*=e^{S^*}\sqrt{\pi S^*}\left[1-\operatorname{erf}\left(\sqrt{S^*}\right)\right] \tag{12}$$

and

$$m_{c,a}^*\left(t_p^*\to\infty\right)=m_{c,lim}^*=\frac{m_{c,lim}\,J_0k_c}{c_b}=\frac{e^{S^*}}{\sqrt{S^*}}\Gamma\left(3/2,S^*\right)-1 \tag{13}$$

where $J_{lim}$ is the value of the limiting or steady-state permeate flux and $m_{c,lim}$ is the steady-state value of the cake mass.

The three parameters of the model can be estimated as follows: The membrane resistance $R_m$ can be determined from the value of the initial flux $J_0$ and Eq. (6), while the dimensionless surface-renewal rate $S^*$ can be calculated from the experimental value of $J_{lim}$ and Eq. (12). The surface-renewal rate $S$ can then be obtained by fitting Eq. (8) to experimental, transient permeate-flux data such that the root-mean-square (RMS) deviation between predicted and experimental values of the flux is minimized. Finally, $k_c$ and $\alpha$ can be calculated from Eqs. (1) and (7), respectively.

## Approximate Model

A rudimentary outline of an approximate model that can be derived from the complete model was

given by Hasan *et al*. (2013). This section presents a detailed derivation and discussion of this approximate model.

In some situations, the value of $J_0$ can be high (e.g., a clean membrane), i.e., $J_0 \to \infty$. Equations (8) and (9) then simplify to:

$$J_a\left(t_p\right) = J_{lim}\frac{\operatorname{erf}\left(\sqrt{St_p}\right)}{1-e^{-St_p}} \tag{14}$$

and

$$m_{c,a}\left(t_p\right) = m_{c,lim}\frac{\left[1-\left(2/\sqrt{\pi}\right)\Gamma\left(3/2, St_p\right)\right]}{1-e^{-St_p}} \tag{15}$$

where

$$J_{lim} = \sqrt{\frac{\pi S}{2k_c}} = \sqrt{\frac{\pi S\Delta p}{2\mu c_b \alpha}} \tag{16}$$

and

$$m_{c,lim} = c_b\sqrt{\frac{\pi}{2Sk_c}} = \sqrt{\frac{\pi c_b \Delta p}{2S\mu\alpha}} = J_{lim}\frac{c_b}{S} \tag{17}$$

As Hasan *et al*. (2013) pointed out, Eq. (14) has the same (mathematical) form as the transient permeate flux in cross-flow ultrafiltration (Chatterjee, 2010). The value of $S$ can be obtained from the experimental value of $J_{lim}$ and by fitting Eq. (14) to transient permeate-flux data, after which $\alpha$ can be determined from Eq. (16).

Equation (16) suggests that an increase in the surface-renewal rate $S$ (e.g., caused by an increase in the level of flow instability), an increase in the transmembrane pressure drop $\Delta p$ or a reduction in feed concentration $c_b$ will increase the value of $J_{lim}$, which is expected on physical grounds. According to Eq. (17), increases in $c_b$ and $\Delta p$ will increase $m_{c,lim}$ which, however, can be compensated for by an increase in $S$. At a fixed value of $c_b$, the ratio $m_{c,lim}/J_{lim}$ is inversely proportional to $S$; thus, the introduction of vortices, which will increase $S$, will decrease this ratio.

Equations (16) and (17) also show the crucial importance of both the surface-renewal rate $S$ and specific cake resistance $\alpha$ in governing the values of $J_{lim}$ and $m_{c,lim}$. The introduction of flow instabilities like Dean vortices is expected to increase $S$ while decreasing $\alpha$ (i.e., a looser, less compact cake). In this case, the limiting permeate flux, which is proportional to $\sqrt{S/\alpha}$, may increase significantly, while there will be a smaller influence on the limiting cake mass since the latter is proportional to $\sqrt{1/(S\alpha)}$.

As $St_p \to 0$, i.e., as $S \to 0$ (low flow instability) or as $t_p \to 0$ ("initial period of filtration"), it can be shown that Eqs. (14) and (15) reduce to:

$$J_a\left(St_p \to 0\right) = \sqrt{\frac{2}{k_c t_p}} = \sqrt{\frac{2\Delta p}{\mu c_b \alpha t_p}} \tag{18}$$

and

$$m_{c,a}\left(St_p \to 0\right) = \frac{2}{3}c_b\sqrt{\frac{2t_p}{k_c}} = \frac{2}{3}\sqrt{\frac{2c_b\Delta p t_p}{\mu\alpha}} \tag{19}$$

At $t_p = 0$, Eq. (18) shows that the permeate flux becomes unbounded, which is a consequence of assuming that the initial flux $J_0 \to \infty$ in the derivation of the approximate model. Further, during the initial period of filtration, or for low levels of flow instability, Eqs. (18) and (19) predict that the permeate flux is inversely proportional to the square root of process time $t_p$ while the cake mass grows as the square root of $t_p$ starting from a value of zero at $t_p = 0$. Equations (18) and (19) also show that, for $St_p \to 0$, the permeate flux is inversely proportional to the square root of the feed concentration $c_b$, whereas the cake mass is directly proportional to the square root of $c_b$. The absence of the surface-renewal rate $S$ in Eqs. (18) and (19) is a consequence of the Danckwerts age-distribution function that was assumed to represent the ages of surface elements in the derivation of Eqs. (8) and (9) (see Hasan *et al*., 2013); this distribution approaches a uniform distribution as $St_p \to 0$. As mentioned earlier, the introduction of Dean vortices into the flow field is expected to decrease the specific cake resistance $\alpha$, with a consequent higher permeate flux [Eq. (18)] compared to the situation when no such vortices are present. This can, therefore, lead to greater cake deposition on the membrane surface [Eq. (19)] because of the higher convective flow of solids to it due to the greater permeate flux during the initial period of filtration. This theoretical conclusion will be validated by calculations for the dynamic growth of the cake mass to be presented later. It should be noted that for small values of $S$, the initial period of filtration [when Eqs. (18) and (19) are valid] will be greater compared to the situation when $S$ is large; this is the meaning of the condition $St_p \to 0$.

Although the purpose of introducing Dean vortices into the flow field is to increase permeate flux, the relative magnitudes of the two parameters $\alpha$ and $S$ without and with vortices can lead to complex

behavior of the permeate-flux and cake-mass curves as a function of process time, and, in some situations, the introduction of such vortices can be detrimental. This is primarily due to greater cake compaction because of an increased permeate flow due to vortices immediately after the start of filtration, i.e., during the "initial moments of filtration." More precise definitions of the "initial moments of filtration" and "initial period of filtration" are given in the Appendix, which also presents a qualitative analysis of the behavior of the permeate-flux and cake-mass curves as a function of process time.

In cake filtration, the specific cake resistance $\alpha$ is often expressed by the empirical relation (McCabe *et al*., 1993):

$$\alpha = \alpha_0 \Delta p^n \tag{20}$$

where $\alpha_0$ and $n$ are empirical constants with $n$ being the compressibility coefficient of the cake, which is zero for incompressible sludges and lies between 0.2 and 0.8 for compressible ones (McCabe *et al*., 1993). Substituting Eq. (20) into Eqs. (16) and (17) yields:

$$J_{lim} = \sqrt{\frac{\pi S}{2\mu c_b \alpha_0}} \Delta p^{\frac{1-n}{2}} \tag{21}$$

and

$$m_{c,lim} = \sqrt{\frac{\pi c_b}{2 S \mu \alpha_0}} \Delta p^{\frac{1-n}{2}} \tag{22}$$

The following observations can be drawn from Eqs. (21) and (22): (1) $J_{lim}$ is directly proportional to $\sqrt{S}$, whereas $m_{c,lim}$ is inversely proportional to it; (2) $J_{lim}$ is inversely proportional to $\sqrt{c_b}$ whereas $m_{c,lim}$ is directly proportional to it; (3) both $J_{lim}$ and $m_{c,lim}$ are inversely proportional to $\sqrt{\mu}$ and $\sqrt{\alpha_0}$; and (4) both $J_{lim}$ and $m_{c,lim}$ are directly proportional to $\Delta p^{\frac{1-n}{2}}$. All of these conclusions are in accord with physical intuition. Although the inverse dependency of $m_{c,lim}$ on $\sqrt{\mu\alpha_0}$ may at first sight appear counterintuitive, smaller values of the permeate viscosity $\mu$ and the compressibility coefficient $\alpha_0$ will result in a higher permeate flux, which will lead to greater cake deposition by the convective flow of liquid towards the membrane surface.

For a perfectly incompressible cake ($n$ = 0), Eq. (21) predicts a 0.5 power dependence of the limiting permeate flux $J_{lim}$ on the transmembrane pressure drop $\Delta p$, with the curve of $J_{lim}$ versus $\Delta p$ becoming increasingly flatter with increasing $n$, which is, once again, in accord with physical intuition since for highly compressible cakes, $J_{lim}$ will be much less sensitive to changes in $\Delta p$. We note that for a perfectly incompressible cake (i.e., $n$ = 0), the resistance model used by Mallubhotla and Belfort (1997), which does not include the effect of (axial) liquid flow, predicts the limiting flux to be proportional to $\Delta p$. Thus, assuming all other factors remain constant, in the case of a perfectly incompressible cake, a doubling of the transmembrane pressure drop will double the limiting permeate flux according to the resistance model, but only increase it by a factor of 1.414 according to the surface-renewal model.

## CRITICAL-FLUX MODEL

The general equation of the critical-flux model is given by (Field *et al*., 1995):

$$-\frac{dJ}{dt_p} J^{n_c - 2} = k\left(J - J_{crit}\right) \tag{23}$$

where $k$ is a constant and $n_c$ equals 0, 1, 1.5, and 2 for cake filtration, intermediate blocking, standard blocking, and complete blocking mechanisms, respectively. $J_{crit}$ is the critical flux which is the value of the permeate flux below which a decline of flux with time does not occur, and which depends upon the prevailing hydrodynamics and other factors, whereas $J$ is the process flux at time $t_p$. For comparison with the previously presented surface-renewal model whose dominant fouling mechanism was assumed to be cake accumulation on the membrane surface, which was the most likely cause for permeate-flux decline in the experiments of Mallubhotla and Belfort (1997) (to be discussed later), only the case for $n_c$ = 0 (i.e., cake filtration) will be considered here. For $n_c$ = 0, Eq. (23) reduces to:

$$-\frac{1}{J^2}\frac{dJ}{dt_p} = k\left(J - J_{crit}\right) \tag{24}$$

whose solution, subject to the initial condition that at $t_p$ = 0, $J = J_0$, is (Field *et al*., 1995):

$$kt_p = \frac{1}{J_{crit}^2}\left[ ln\left(\frac{J}{J_0}\left(\frac{J_0 - J_{crit}}{J - J_{crit}}\right)\right) - J_{crit}\left(\frac{1}{J} - \frac{1}{J_0}\right)\right] \tag{25}$$

which is an implicit equation for the permeate flux $J$ as a function of process time $t_p$, in contrast to the explicit form for the surface-renewal model [see Eqs. (8) and (14)]. It can be seen that Eq. (25) contains three parameters: $J_0$, $J_{crit}$ and $k$. $J_0$ can be expressed in terms of $R_m$ and $\Delta p$ through Eq. (6). According to Eq. (24), $dJ/dt_p = 0$ at $J = J_{crit}$, and, since this is expected to occur as $t_p \rightarrow \infty$, it has been assumed in this work that $J_{crit}$ is equal to the experimental value of the limiting or steady-state flux $J_{lim}$ (see also Arnot *et al*., 2000). The third parameter $k$ can then be obtained from the slope of a plot of the right-hand-side of Eq. (25) as a function of $t_p$. It is to be noted that $k$ and $J_{crit}$ can be expressed in terms of the following more fundamental parameters (Field *et al*., 1995):

$$k = \frac{\alpha K_{cake}}{J_0 R_m} \tag{26}$$

and

$$J_{crit} = \frac{E}{K_{cake}} \tag{27}$$

Here, $K_{cake}$ is a cake-filtration constant (a function of certain physical properties) and $E$ is the rate of cake erosion per unit area. Thus, according to Eq. (27) [which is analogous to Eqs. (12) and (16) of the surface-renewal model], an increase in $E$ (say, due to an increase in the liquid velocity or level of flow instability) and a decrease in $K_{cake}$ will cause an increase in $J_{crit}$ (i.e., the limiting or steady-state flux). Unfortunately, Field *et al.* (1995) did not provide a definition for $K_{cake}$, which precluded calculating values of the basic quantities $\alpha$, $E$, and $K_{cake}$ from values of $J_{crit}$ and $k$, which can be obtained from experimental permeate-flux data as discussed earlier. From Eqs. (26) and (27) it follows that:

$$E_{mod} = \alpha E = k J_0 J_{crit} R_m \tag{28}$$

Thus, although $\alpha$ and $E$ cannot be separately determined, their product $E_{mod}$, which is a modified cake erosion parameter, can be calculated.

## A BRIEF SUMMARY OF THE EXPERIMENTAL METHODOLOGY OF MALLUBHOTLA AND BELFORT (1997)

As mentioned earlier, Belfort and co-workers investigated the use of Dean vortices in cross-flow membrane filtration. Such vortices reduce concentration polarization and solids buildup at the membrane-liquid interface, which greatly enhance the flux of permeate compared to operation without vortices. In what follows, both the complete and approximate surface-renewal models presented earlier are correlated against the dynamic permeate-flux data reported in Figure 3 of the paper by Mallubhotla and Belfort (1997). These data were obtained from CFMF runs using a polysulfone membrane with a nominal pore size of 0.2 μm and a feed suspension containing polydispersed particles (average nominal diameter $d_p$ = 25 μm, density $\rho_p$ = 1052 kg/m$^3$) that was made by suspension polymerization of styrene-divinyl-benzene (S/DVB). The particle volume fraction $\phi$ in the suspension was 0.0015 (base case), which upon multiplying by the particle density $\rho_p$ yields a value of 1.578 kg/m$^3$ for the bulk concentration $c_b$ of particles in the suspension. These were the only dynamic permeate-flux data that we could find on CFMF with Dean vortices in the publications of Belfort and co-workers that were cited previously. It should be mentioned that such data are necessary for estimating the parameters of the surface-renewal model (i.e., $R_m$, $S$ and $\alpha$ of the complete model, and $S$ and $\alpha$ of the approximate model).

We note that the vortex intensity is expressed as a Dean number ratio $D$, defined as $De/De_c$ where the Dean number $De$ can be interpreted as the ratio of centrifugal to viscous forces (Mallubhotla and Belfort, 1997). Here, $De = (2du/\vartheta_s)\sqrt{2d/r_c}$, where $d$ is the half channel height ($2d = R_2 - R_1$), $u$ is the mean axial liquid velocity, $\vartheta_s$ is the kinematic viscosity of the feed suspension, $r_c$ is the centerline radius of the curved channel (see below), while $R_1$ and $R_2$ are the radii of curvature of the inner and outer walls of the curved channel, respectively. $De_c$ is the critical value of the Dean number [equal to 35.71 in the experimental system of Mallubhotla and Belfort (1997)] above which the fluid becomes unstable and vortices are produced. Their test cell, which had an active surface area $A$ of 48.4 cm$^2$, consisted of a thin channel with width $W$, height $H$ and length $L$ of 63.5, 1.6 and 76.2 mm, respectively. There was a 180º U-bend ($R_1$ = 61.9 and $R_2$ = 63.5 mm) through which the feed flowed before it entered the test cell; this arrangement generated Dean vortices in the flow field. By reversing the flow direction, they could conduct their CFMF operation in the absence of such vortices. The experiments were performed at a liquid velocity $u$ = 0.57 m/s, transmembrane pressure drop $\Delta p$ = 69.8 kPa and Dean number ratio $D$ = 4.77 (base case).

There is controversy in the literature regarding the meaning to be attributed to the initial permeate flux $J_0$, and thus the value of the membrane resistance

$R_m$ calculated from Eq. (6). As discussed by Hasan *et al*. (2013), in conventional cake-filtration theory, no complete analysis of the buildup of the (initial) resistance of the filter cloth is possible since this resistance will depend on how the pressure is developed and on the support geometry; it is therefore usual to combine the resistance of the cloth with that of the first few layers of deposited particles, which have a tendency to block the pores of the cloth (Richardson *et al*., 2002). The value of $R_m$ will then reflect the combined resistance of the membrane and those particle layers that deposit on it during the initial moments of filtration. In the microfiltration of sugar-maple wood extract, Hasan *et al*. (2011) observed a significant difference between values of the initial permeate flux $J_0$ and the clean-water flux, which they attributed to a difference in viscosity. Huang and Morrissey (1998) found that $J_0$, which they called the apparent initial permeate flux, depended on the feed concentration — the higher this concentration, the lower was the initial flux. According to them, it is difficult to measure the true initial permeate flux since it is not possible to stabilize the system pressure instantaneously as the feed is pumped into the filter. According to Koltuniewicz (1992), the first measurement point can be obtained only after some 'lag' time that depends upon the measurement technique; he recommended that pure solvent permeability measurements, after correction for the osmotic pressure effect, be used to calculate $J_0$ in the case of ultrafiltration. This points to uncertainty associated with experimental data of permeate flux near the beginning of filtration. In light of these considerations, it is (generally) best to treat $R_m$ as an empirical parameter, which would also include any resistance to flow in the pipes to and from the filter (McCabe *et al*., 1993). In the modeling of microfiltration, Arnot *et al*. (2000) also used $J_0$ as an adjustable parameter in order to minimize experimental errors in the initial flow rate measurement — although they found that in most cases it was not significantly different from the clean-water flux under equivalent operating conditions.

As mentioned earlier, the permeate-flux data of Mallubhotla and Belfort (1997) that will be analyzed in this work were obtained with a feed suspension that consisted of polydisperse particles of S/DVB having an average nominal diameter of 25 μm. Measurement of the number and volume size distributions by a Coulter counter revealed that the highest frequency of particles occurred between 2 and 10 μm (Mallubhotla and Belfort, 1997). Since these values are much greater than the nominal pore size of 0.2 μm of the polysulfone membrane used in their experimental work, it can be safely conjectured that there was minimal or negligible pore blocking of the membrane in their microfiltration experiments. We therefore assumed that the value of the initial permeate flux $J_0$ in Eq. (6) could be calculated from the pure water flux, which was equal to 221 L/(m$^2$ h). Since Mallubhotla and Belfort, (1997) did not report the experimental temperature, a temperature of 20 ºC was assumed, at which the viscosity of water is estimated to be 0.0011 kg/(m s) (Perry *et al*., 1984). This value, the pure water flux value and the value of the transmembrane pressure drop $\Delta p$ (= 69.8 kPa) were used in Eq. (6) to estimate the membrane resistance $R_m$ as $9.6 \times 10^{11}$ m$^{-1}$. In the calculations, the viscosity of the filtrate was also assumed to be 0.0011 kg/(m s).

A brief summary of the experimental parameters of Mallubhotla and Belfort (1997) is provided in Table 1 and the reader is referred to their paper for a schematic of the experimental apparatus, detailed discussion of the experimental conditions and procedures, and interpretation of the results.

**Table 1: Experimental parameters of Mallubhotla and Belfort (1997).**[a]

| Parameter | Description or value |
|---|---|
| Membrane type | polysulfone with a 0.2 μm pore size |
| Particle type in the feed suspension | styrene-divinyl-benzene (S/DVB) |
| Particle average nominal diameter ($d_p$) | 25 μm |
| Particle density ($\rho_p$) | 1052 kg/m$^3$ |
| Particle volume fraction ($\phi$) | 0.0015 (base case) |
| Active area of the test cell ($A$) | 48.4 cm$^2$ |
| Height of the test cell ($H$) | 1.6 mm |
| Length of the test cell ($L$) | 76.2 mm |
| Width of the test cell ($W$) | 63.5mm |
| Critical Dean number ($De_c$) | 35.71 |
| Dean number ratio ($D = De/De_c$) | 4.77 (base case) |
| Transmembrane pressure drop ($\Delta p$) | 69.8 kPa |
| Liquid velocity ($u$) | 0.57 m/s |
| Pure water flux | 221 L/(m$^2$ h) |

[a] An experimental temperature of 20 ºC was assumed in the calculations.

## RESULTS AND DISCUSSION

### Surface-Renewal Model

### Complete Model

Figure 3 shows the fit of the complete model to the transient permeate-flux data obtained by Mallubhotla and Belfort (1997) for CFMF runs both without and with Dean vortices. It is observed that: (1) The experimental permeate flux declines with

process time and eventually attains a steady-state value as predicted by theory, (2) the experimental permeate flux with Dean vortices is significantly greater and approaches the limiting or steady-state value faster when compared to that without vortices, and (3) there is a fairly good fit of the model [Eq. (8)] to the experimental data, both in the absence and presence of vortices.

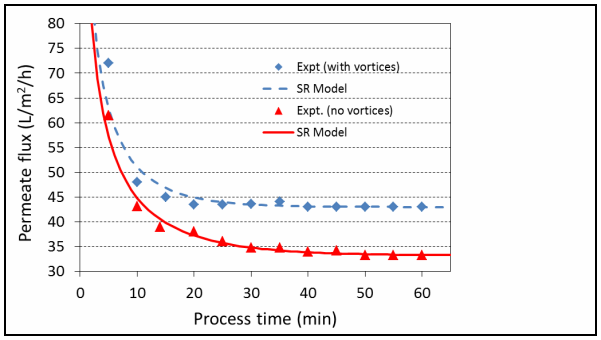


**Figure 3:** Comparison of the surface-renewal complete model [Eq. (8)] and experimental (Figure 3 of Mallubhotla and Belfort, 1997) permeate fluxes in the microfiltration of a S/DVB particulate suspension. Experimental and model parameters are provided in Tables 1 and 2, respectively. SR denotes surface renewal.

With no vortices, the average root-mean-square (RMS) deviation between the theoretical and experimental permeate fluxes is 2.6% with the surface-renewal rate $S$ being estimated at $1.5 \times 10^{-3}$ s$^{-1}$. The specific cake resistance $\alpha$, which measures the resistance offered by the accumulated material on the membrane surface to the flow of permeate, and which depends on the packing density and nature of the cake, is estimated to be $8.42 \times 10^{14}$ m kg$^{-1}$, while the limiting or steady-state cake mass $m_{c,lim}$, calculated from Eq. (13), is found to be $9.70 \times 10^{-3}$ kg m$^{-2}$. If this value is multiplied by the value of the active area $A$ of the test cell (Table 1), the total mass of accumulated solids on the membrane is calculated to be 47 mg when the steady-state is reached.

The introduction of flow instabilities due to Dean vortices increased the surface-renewal rate by 53% ($S = 2.3 \times 10^{-3}$ s$^{-1}$), decreased the specific cake resistance by 14.5% ($\alpha = 7.20 \times 10^{14}$ m kg$^{-1}$), with a consequent increase in the limiting permeate flux $J_{lim}$ by 30% and a decrease in the limiting cake mass by 15.5% ($m_{c,lim} = 8.19 \times 10^{-3}$ kg m$^{-2}$, total accumulation of solids on the membrane surface at steady-state = 39.7 mg). The RMS error of fit between theory and experiment is 4.3%, which is higher than the value of 2.6% obtained for the case when vortices were absent.

Figure 4 exhibits the predicted, age-averaged cake mass $m_{c,a}$, [calculated from Eq. (9)] as a function of process time $t_p$ in the absence and presence of vortices. Both curves start at a value of zero and approach the corresponding steady-state values reported earlier as the filtration progresses. During the first 10 min, the mass of cake deposited on the membrane wall is greater in the presence of vortices compared to that in the absence of vortices. Thereafter, the situation is reversed, with the growth of cake in the absence of vortices gradually outpacing that in the presence of vortices. This behavior was theoretically anticipated earlier, although the discussion was presented in the context of the approximate model.

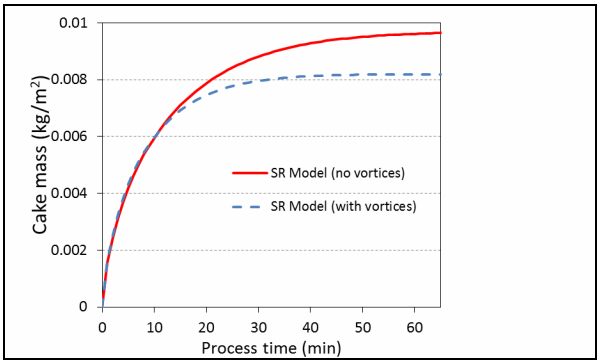


**Figure 4:** Predicted cake buildup with process time according to the surface-renewal complete model [Eq. (9)] in the microfiltration of a S/DVB particulate suspension. Experimental and model parameters are provided in Tables 1 and 2, respectively. SR denotes surface renewal.

## Approximate Model

Calculations made with the approximate model show the same qualitative features as the complete model with somewhat different values estimated for the model parameters. Figure 5 shows the fit of the approximate model [Eq. (14)] to the experimental permeate-flux data of Mallubhotla and Belfort (1997) without and with Dean vortices. With no vortices, the RMS deviation between the theoretical and experimental permeate fluxes is 2.3%, with the surface-renewal rate $S$ estimated at $1.6 \times 10^{-3}$ s$^{-1}$. The specific cake resistance $\alpha$ is estimated to be $1.10 \times 10^{15}$ m kg$^{-1}$ and the limiting cake mass $m_{c,lim}$, calculated from Eq. (17), is found to be $9.1 \times 10^{-3}$ kg m$^{-2}$ (total accumulation of solids on the membrane surface at steady-state = 44 mg).

With the introduction of Dean vortices, the surface-renewal rate $S$ increased by 50% to $2.4 \times 10^{-3}$ s$^{-1}$, the specific cake resistance $\alpha$ decreased by 10.5% to

$9.87 \times 10^{14}$ m kg$^{-1}$, the limiting permeate flux $J_{lim}$ increased by 30%, and the limiting cake mass $m_{c,lim}$ decreased by 13.7% to $7.85 \times 10^{-3}$ kg m$^{-2}$ (total accumulation of solids on the membrane surface at steady-state = 38 mg). The RMS error of fit between theory and experiment is 3.9%, compared to 2.3% obtained for the case without vortices.

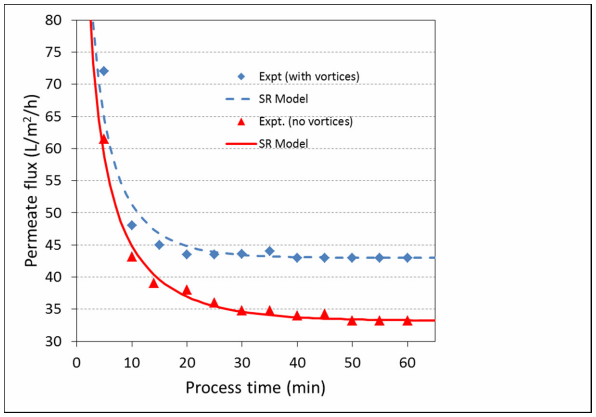


**Figure 5:** Comparison of the surface-renewal approximate model [Eq. (14)] and experimental (Figure 3 of Mallubhotla and Belfort, 1997) permeate fluxes in the microfiltration of a S/DVB particulate suspension. Experimental and model parameters are provided in Tables 1 and 2, respectively. SR denotes surface renewal.

Figure 6 shows the dynamic behavior of the theoretical, age-averaged cake mass $m_{c,a}$, [calculated from Eq. (15)] as a function of process time in the absence and presence of vortices. This behavior is similar to that observed for the complete model.

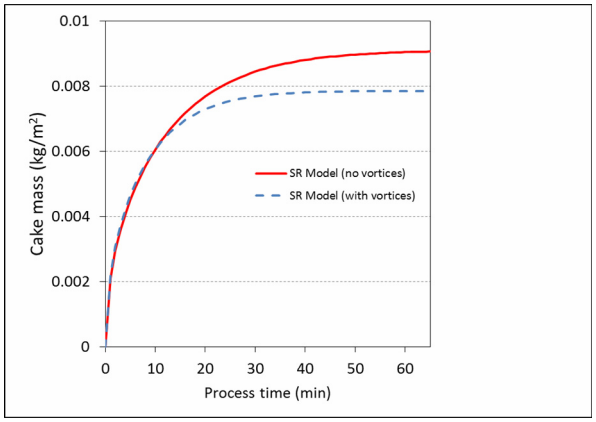


**Figure 6:** Predicted cake buildup with process time according to the surface-renewal approximate model [Eq. (15)] in the microfiltration of a S/DVB particulate suspension. Experimental and model parameters are provided in Tables 1 and 2, respectively. SR denotes surface renewal.

Using subscripts 1 and 2 to denote the situations without and with vortices, respectively, Table 2 gives $S_2/S_1 = 1.5$ and $\alpha_1/\alpha_2 = 1.11$ for the approximate model. Since $\alpha_1/\alpha_2 < S_2/S_1$, the behavior of the permeate flux and cake buildup on the membrane surface as a function of process time shown in Figures 5 and 6 corresponds to Figures A1(a) and A1[b(ii)], respectively, in the Appendix.

For the benefit of the reader, the model parameters, along with the RMS deviations between theory and experiment, are gathered together in Table 2 for both the complete and approximate models.

**Table 2: Parameter values of the surface-renewal model and RMS deviations between theory and experiment (Figures 3 and 5).**

| Parameter | Without vortices | | With vortices | |
|---|---|---|---|---|
| | ***Complete model*** | ***Approx. model*** | ***Complete model*** | ***Approx. model*** |
| $R_m$ (m$^{-1}$) | $9.6 \times 10^{11}$ | – | $9.6 \times 10^{11}$ | – |
| $S$ (s$^{-1}$) | $1.5 \times 10^{-3}$ | $1.6 \times 10^{-3}$ | $2.3 \times 10^{-3}$ | $2.4 \times 10^{-3}$ |
| $\alpha$ (m kg$^{-1}$) | $8.42 \times 10^{14}$ | $1.10 \times 10^{15}$ | $7.20 \times 10^{14}$ | $9.87 \times 10^{14}$ |
| RMS deviation (%) | 2.6 | 2.3 | 4.3 | 3.9 |

Mallubhotla and Belfort (1997) also reported results on the limiting permeate flux and flux enhancement (due to Dean vortices) as a function of transmembrane pressure drop under different experimental conditions. However, we were unable to use these data to estimate values of the surface-renewal rate $S$ and compressibility constants of the cake ($\alpha_0$ and $n$) because of their steady-state nature and their unavailability at low values of the transmembrane pressure drop (i.e., below 36 kPa). In what follows, we present an approximate analysis that will indicate the relationship between the change in the quantity $\omega = S/\alpha_0$ (due to vortices) and the Dean number ratio $D$, which, as mentioned earlier, is a measure of vortex intensity.

Using subscripts 1 and 2 to denote the situations without and with vortices, respectively, the limiting flux enhancement $FE$ as a function of transmembrane pressure drop $\Delta p$ can be obtained from Eq. (21) as:

$$FE = \frac{J_{lim,2} - J_{lim,1}}{J_{lim,1}} = \sqrt{\frac{S_2/\alpha_2}{S_1/\alpha_1}} - 1 = \sqrt{\frac{S_2/\alpha_{02}}{S_1/\alpha_{01}}} \Delta p^{\frac{n_1 - n_2}{2}} - 1 = \sqrt{\frac{\omega_2}{\omega_1}} \Delta p^{\frac{n_1 - n_2}{2}} - 1 \tag{29}$$

where $\omega_1 = S_1/\alpha_{01}$ and $\omega_2 = S_2/\alpha_{02}$ while $J_{lim,1}$ and $J_{lim,2}$ are the limiting permeate fluxes without and

with vortices, respectively. According to Eq. (29), the flux enhancement will be much less sensitive to the transmembrane pressure drop than the individual limiting permeate fluxes [see Eq. (21)]. Figure 6 in the paper of Mallubhotla and Belfort (1997) shows the behavior of *FE* as a function of $\Delta p$ (in the range 36−74 kPa) at four different levels of *D* (obtained by varying the liquid velocity) at a S/DVB particle volume fraction $\phi$ = 0.00075 for a 0.2 µm polypropylene membrane. Beyond a value of 36 kPa (the lowest $\Delta p$ at which *FE* data are available), *FE* increases only weakly with $\Delta p$; i.e., the curve of *FE* versus $\Delta p$ flattens out. This implies that $n_1 \approx n_2$, i.e., vortices do not affect the compressibility coefficient of the cake, which reduces Eq. (29) to:

$$\frac{\omega_2}{\omega_1} = \left(1 + FE\right)^2 \tag{30}$$

where *FE* is now to be interpreted as the average flux enhancement over the range of $\Delta p$ (i.e., 36−74 kPa) at a given value of *D*. Average values of *FE* over the $\Delta p$ range can be estimated from Figure 6 of Mallubhotla and Belfort (1997) at different values of *D*; such estimates are reported in Table 3. The average absolute deviation of the individual *FE* values from the average *FE* value at a particular *D* value is also shown in this table; this will give an idea of the magnitude of the error involved in making the assumption that led to Eq. (30). As may be seen, the maximum average deviation is 14.5% at *D* = 5.4. The factor $\omega_2 / \omega_1 - 1$ can be calculated from the average *FE* value using Eq. (30); values of this factor are shown in Table 3 and plotted as a function of $(D-1)$ in Figure 7. We observe that the data fall fairly well on a straight line and can be expressed as:

$$\frac{\omega_2}{\omega_1} - 1 = K\left(D - 1\right) \tag{31}$$

where *K* = 0.182. It should be noted that vortices are only generated when *D* is larger than 1; thus the line in Figure 7 passes through the origin. Equation (31) clearly shows that the fractional increase in the ratio $S / \alpha_0$ because of vortices is directly related to the vortex intensity (represented by *D*).

**Table 3: Average limiting flux enhancement (*FE*) as a function of the Dean number ratio (*D*). Data are derived from Figure 6 of Mallubhotla and Belfort (1997) for a S/DVB particle volume fraction $\phi$ = 0.00075 and a 0.2 µm polypropylene membrane over a transmembrane pressure drop ($\Delta p$) range of 36−74 kPa. Other experimental parameters are shown in Table 1.**

| Dean number ratio *D* | Liquid velocity *u* (m/s) | Average limiting flux enhancement *FE* | Average absolute deviation of individual *FE*s from average *FE* (%) | $\omega_2 / \omega_1$ - 1 [calculated from Eq. (30)] |
|---|---|---|---|---|
| 1.00 | 0.119[a] | 0[b] | – | 0 |
| 4.02 | 0.480 | 0.23 | 10 | 0.50 |
| 4.71 | 0.562 | 0.28 | 8.4 | 0.64 |
| 5.40 | 0.644 | 0.35 | 14.5 | 0.83 |
| 6.10 | 0.728 | 0.40 | 7.2 | 0.96 |

[a] calculated [b] assumed

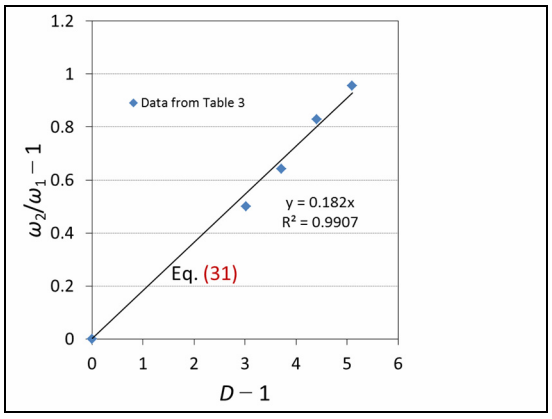


**Figure 7:** Behavior of the factor $(\omega_2 / \omega_1 - 1)$ as a function of $(D-1)$ The solid line is a fit of Eq. (31) to the data in Table 3.

Mallubhotla and Belfort (1997) also studied the effect of particle concentration on the steady-state or limiting flux enhancement *FE*. For example, the data presented in Table 4, which were extracted from Figure 8 of their paper, show that *FE* increases as the particle volume fraction $\phi$ is raised from a value of zero, reaches a maximum of 27% at $\phi = 0.0015$, and then again drops to zero at $\phi = 0.002$. We note the 3% discrepancy between the *FE* value of 27% at $\phi = 0.0015$ given in Table 4 and the value of 30% (at the same value of $\phi$) that was mentioned previously in the discussion of Figures 3 and 5. The likely cause for this discrepancy is human subjectivity in extracting the data for the limiting flux (Figure 3 or Figure 5) from Figure 3 in the paper of Mallubhotla and Belfort (1997). These authors attributed the flux loss to compression of the deposited cake and increased viscosity and particle-particle interactions near the membrane surface as $\phi$ is increased. This, however, does not explain the increase in *FE* as $\phi$ varies from zero to 0.0015. We now offer a hypothesis for the experimentally observed initial increase and subsequent decrease of *FE* as $\phi$ as raised (Table 4). As $\phi$ is increased, the nature of the cake will change, i.e., the specific cake resistance is expected to increase, both in the absence and presence of vortices. Although the effect of particle concentration $c_b$ ($=\phi\,\rho_p$) does not explicitly appear in Eq. (29), it is indirectly manifested through the magnitudes of the specific cake resistances $\alpha_1$ and $\alpha_2$, with the latter also depending on the strength of the vortex intensity (reflected by the value of $S_2$). At a fixed value of the Dean number ratio *D*, the value of $S_2 / S_1$ (> 1) would be fixed (assuming that the surface-renewal rate is independent of particle concentration since it is a hydrodynamic parameter). As $\phi \to 0$ (i.e., $c_b \to 0$ or $k_c \to 0$), it can be shown from Eqs. (6) and (12) in the paper of Hasan *et al*. (2013) that the permeate flux becomes independent of time and the surface-renewal rate (i.e., becomes equal to the initial flux $J_0$). From this it follows that $FE \to 0$, which also implies that cake buildup with and without vortices would be the same, and would approach zero as shown by Eqs. (8) and (22) in the paper of Hasan *et al*. (2013). Table 4 also reports numerical values of the ratio $\alpha_1/\alpha_2$ as a function of *FE* calculated from Eq. (29) by using a value of $S_2/S_1 = 1.5$, which was obtained from Table 2 (approximate model). As $\phi$ increases from a value of zero, $\alpha_1/\alpha_2$ reaches a maximum value of 1.08 at $\phi = 0.0015$ (*FE* = 0.27) and then drops to 0.67 at $\phi = 0.002$ (*FE* = 0). The increase in *FE* implies that, although both $\alpha_1$ and $\alpha_2$ increase with $\phi$, $\alpha_1$ increases at a greater rate than $\alpha_2$ ; in this region, *FE* increases with $\phi$. But this increase occurs only up to a certain value of $\phi$, beyond which the trend is reversed, and, as $\phi$ is increased further, $\alpha_2$ increases at a greater rate than $\alpha_1$. In this region, *FE* decreases as $\phi$ increases, i.e., vortices become less and less effective, with *FE* becoming zero when a threshold value of $\phi$ is crossed (0.002 in Table 4). On the ascending side of the *FE* versus $\phi$ plot [Figure 8 in the paper of Mallubhotla and Belfort, 1997], $\alpha_1 / \alpha_2 \approx 1$ at $\phi = 0.0005$ where *FE* = 0.22 (Table 4), whereas on the descending side, these same values of $\alpha_1/\alpha_2$ and *FE* occur at approximately $\phi = 0.00165$. Thus, within the range of $0.0005 < \phi < 0.00165$, $\alpha_1/\alpha_2 > 1$ and vortices are especially effective. Outside this range, $\alpha_1/\alpha_2 < 1$, i.e., vortices increase the specific cake resistance. We attribute this behavior to greater cake compaction (causing a reduction in cake porosity) due to a heightened permeate flux in the presence of vortices immediately after the beginning of filtration, with the compaction effect being much more severe at higher values of $\phi$. Thus, in the ascending part of the *FE* versus $\phi$ plot, a change in $\phi$ of 0.0015 leads to an increase of 27% in *FE*, whereas in the descending part of the plot, a change in $\phi$ of only 0.0005 leads to the same amount of decrease in *FE*. It can be observed from Eq. (29) that another critical factor governing the behavior of *FE* is $S_2/S_1$. Since this factor will be greater than 1 when vortices are introduced into the flow field, there will be some flux enhancement even when $\alpha_1 < \alpha_2$, with the enhancement being especially significant when $\alpha_1 > \alpha_2$, which will occur in a specific particle volume fraction range [$0.0005 < \phi < 0.00165$ in the experiments of Mallubhotla and Belfort, 1997]. Thus, there is a range of $\phi$ within which the use of vortices is advantageous and outside of which the need for them disappears (Mallubhotla and Belfort, 1997). Table 4 also lists the number of the figure in the Appendix that corresponds to each individual case.

It was assumed in the preceding discussion that the specific cake resistance $\alpha$ is a function of the feed concentration $c_b$. For a cake consisting of rigid individual particles, this is not expected to be true and, in such a case, both $\alpha_1$ and $\alpha_2$ (and thus their ratio) will be independent of the feed concentration. Also, in this case, $\alpha_1/\alpha_2 > 0$ (no cake compaction) and thus *FE* > 0 [Eq. (29)], which will be independent of particle concentration in the feed, and which corresponds to

Case 1 in the Appendix. However, for a compressible cake formed from a flocculated suspension, the resistance of the cake will be governed by floc properties, the method used in preparing the feed suspension and age and temperature of the material constituting it, floc distortion and breakage due to forces within the cake, and variation of cake properties within the cake layer (McCabe *et al*., 1993). Also, due to consolidation and creep effects, the local (and average) value of $\alpha$ can vary with process time and the introduction of fluid shear (e.g., vortices) will restrict the suspension of flocs with different material properties compared to those in the absence of shear (Kovalsky *et al*., 2009). These effects will be different for suspensions of differing feed concentrations, which will be manifested as a dependence of $\alpha$ on $c_b$. It becomes evident that the surface-renewal model used in this work, which tacitly assumes that, during the initial moments of filtration, a complete cake layer is formed on the membrane surface, whose resistance (represented by $\alpha$) thereafter does not change with time, is a highly idealized picture of a very complex process. This is a usual feature of a scientific model, which is an interpretative and partial description of a phenomenon and which facilitates access (perceptual and intellectual) to that phenomenon (Bailer-Jones, 2009).

**Table 4: Limiting flux enhancement (*FE*) as a function of particle volume fraction ($\phi$) with a S/DVB particulate suspension at a Dean number ratio (*D*) = 4.77 and transmembrane pressure drop ($\Delta p$) = 69.8 kPa for a 0.2 μm polysulphone membrane. Liquid velocity (*u*) = 0.57 m/s and critical Dean number ($De_c$) = 35.71. Data were derived from Figure 8 of Mallubhotla and Belfort (1997).**

| Particle volume fraction $\phi$ | Limiting flux enhancement *FE* | $\alpha_1/\alpha_2$ [calculated from Eq. (29)] | Figure No. |
|---|---|---|---|
| 0.0 | 0 | - | - |
| 0.0005 | 0.22 | 0.99 ≈ 1 | A2 [a and b] |
| 0.0015 | 0.27 | 1.08 | A1 [a and b(ii)] |
| 0.0020 | 0 | 0.67 | A3 [a and b(iii)] |
| 0.0025 | 0 | - | - |

The average values of *S* calculated from Table 2 are $1.55 \times 10^{-3}$ s$^{-1}$ (without vortices) and $2.35 \times 10^{-3}$ s$^{-1}$ (with vortices), which is an increase of 52%. These values of *S* are comparable to those reported previously for cross-flow ultrafiltration and microfiltration (Koltuniewicz and Noworyta, 1994; Chatterjee, 2010; Hasan *et al*., 2013). Hutchinson and Sherwood (1937) studied the absorption of eight different pure gases at 25 ºC in a stirred flask containing water with the gas exposed above the stirred surface. Table 5 shows values of the mass-transfer coefficient $k_L$, which they calculated from dissolved-gas concentration measurements, for hydrogen and oxygen at two different stirrer speeds. Using the theoretical equation $k_L = \sqrt{D_i S}$ (Danckwerts, 1970) where $D_i$ is the diffusion coefficient of the dissolved gas in the liquid, we calculated values of *S* that are also reported in Table 5, along with values of $D_i$ that were estimated from values of the diffusion coefficient of the dissolved gas (in water) at 20 ºC given in Table 3 in the paper of Hutchinson and Sherwood (1937) and using the Wilke-Chang correlation (Perry *et al*., 1984) to correct them to 25 ºC. As the stirrer speed changes from 171 RPM (revolutions per minute) to 1025 RPM, *S* varies from $1.86 \times 10^{-2}$ s$^{-1}$ to $1.76 \times 10^{-1}$ s$^{-1}$ for hydrogen and $3.28 \times 10^{-2}$ s$^{-1}$ to $2.13 \times 10^{-1}$ s$^{-1}$ for oxygen. Since *S* is a hydrodynamic parameter, which should be independent of $D_i$, it can be speculated that the difference in the values of *S* between hydrogen and oxygen at a given RPM arises from uncertainty in the value of $D_i$. The average values of *S* at 171 and 1025 RPM are $2.57 \times 10^{-2}$ s$^{-1}$ and $1.94 \times 10^{-1}$ s$^{-1}$, respectively, which indicates an increase of 659% for a change in RPM of 500%, and which also indicates that *S* varies with the RPM raised to a power of 1.13. The values of *S* derived from the absorption data of Hutchinson and Sherwood (1937) are about one to two orders of magnitude greater than those for cross-flow microfiltration, as found in this work. It can be conjectured that high values of *S* can be obtained in a rotating-disk membrane module such as the one used by Sarkar *et al*. (2011), which will dramatically enhance the permeate flux.

From standard mass-transfer coefficient correlations for flow in a tube, Hasan *et al.* (2013) deduced that *S* (in the absence of vortices) varies with the liquid (i.e., feed) velocity *u* raised to a power that ranges from 0.66−1.75 as the flow changes from laminar to turbulent. According to Eq. (16), the limiting or steady-state permeate flux in cross-flow microfiltration is proportional to $S^{0.5}$, a result that also holds for cross-flow ultrafiltration (Chatterjee, 2010). The limiting flux should therefore be proportional to $u^{0.33}$ for laminar flow and $u^{0.875}$ in the case of turbulent flow. This conclusion, as pointed out by Hasan *et al.* (2013), agrees closely with the observation made by Rudolph and MacDonald (1994) that, for modules that operate in the laminar flow regime, the flux increases as the one-third power of the tangential flow rate (or shear), while for devices operat-

ing in the turbulent flow regime, the flux increases in proportion to the tangential flow rate. It should also be noted that, in the case of ultrafiltration, according to Cheryan (1986), the permeate flux is proportional to $u^{0.3}$ to $u^{0.6}$ for laminar-flow units and $u^{0.8}$ to $u^{1.2}$ for turbulent-flow systems.

**Table 5: Values of the surface-renewal rate ($S$) calculated from the absorption data of pure gases at 25 ºC in a stirred flask containing water with the gas exposed above the stirred surface. Values of the mass-transfer coefficient ($k_L$) and diffusion coefficient ($D_i$) were derived from the paper of Hutchinson and Sherwood (1937).**

| Type of gas | RPM | |
|---|---|---|
| *Hydrogen* | 171 | 1025 |
| $k_L$ (m s$^{-1}$) | $1.06 \times 10^{-5}$ | $3.25 \times 10^{-5}$ |
| $D_i$ (m$^2$ s$^{-1}$) | $6.00 \times 10^{-9}$ | $6.00 \times 10^{-9}$ |
| $S$ (s$^{-1}$) [$= k_L^2 / D_i$] | $1.86 \times 10^{-2}$ | $1.76 \times 10^{-1}$ |
| *Oxygen* | 171 | 1025 |
| $k_L$ (m s$^{-1}$) | $8.33 \times 10^{-6}$ | $2.12 \times 10^{-5}$ |
| $D_i$ (m$^2$ s$^{-1}$) | $2.12 \times 10^{-9}$ | $2.12 \times 10^{-9}$ |
| $S$ (s$^{-1}$) [$= k_L^2 / D_i$] | $3.28 \times 10^{-2}$ | $2.13 \times 10^{-1}$ |

## Critical-Flux Model

Finally, the results for the critical-flux model are displayed in Figure 8 (permeate flux) with the model parameters shown in Table 6. With no vortices, the average RMS error between the critical-flux and experimental permeate fluxes is 4.5% [compared to 2.6 and 2.3% for the complete and approximate surface-renewal models, respectively], while with vortices the error increases to 5.1% [compared to 4.3 and 3.9% for the complete and approximate surface-renewal models, respectively].

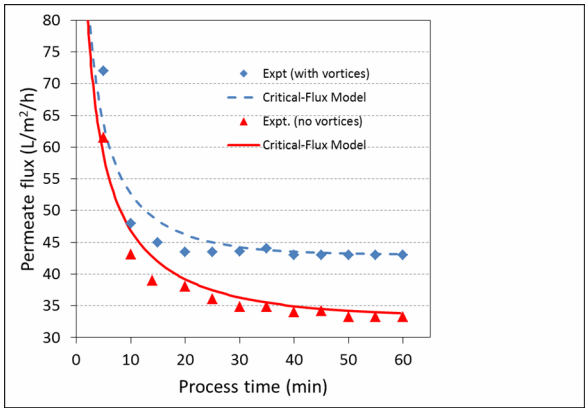


**Figure 8:** Comparison of the critical-flux model [Eq. (25)] and experimental (Figure 3 of Mallubhotla and Belfort, 1997) permeate fluxes in the microfiltration of a S/DVB particulate suspension. Experimental and model parameters are provided in Tables 1 and 6, respectively.

As can be seen by comparing Figure 8 with Figures 3 or 5, the quality of the fit of the critical-flux model to the experimental permeate-flux data is not as good as that of the surface-renewal model. Vortices cause an almost 30% increase in the modified cake erosion parameter $E_{mod}$ (Table 6).

**Table 6: Parameter values of the critical-flux model and RMS deviations between theory and experiment (Figure 8).**

| Parameter | Without vortices | With vortices |
|---|---|---|
| $R_m$ (m$^{-1}$) | $9.6 \times 10^{11}$ | $9.6 \times 10^{11}$ |
| $J_{crit}$ (m s$^{-1}$) | $9.222 \times 10^{-6}$ | $1.194 \times 10^{-5}$ |
| $E_{mod}$ (m s$^{-3}$) | $5.43 \times 10^{9}$ | $7.04 \times 10^{9}$ |
| RMS deviation (%) | 4.5 | 5.1 |

## CONCLUSIONS

The introduction of flow instabilities into a microfiltration process can dramatically change several elements such as the surface-renewal rate, permeate flux, specific cake resistance, and cake buildup on the membrane surface in a positive way. In this work, a recently developed surface-renewal model for constant-pressure, cross-flow microfiltration (Hasan *et al*., 2013) was applied to the permeate-flux data reported by Mallubhotla and Belfort (1997), one set of which included flow instabilities (Dean vortices) while the other set did not. The surface-renewal model has two forms − the complete model and an approximate model, which was derived from the complete model. The complete model has three parameters (membrane resistance, specific cake resistance and surface-renewal rate) while the approximate model has only two (specific cake resistance and surface-renewal rate). These parameters were estimated for the two models by fitting them to the permeate-flux data of Mallubhotla and Belfort (1997). In the case of the complete model, the introduction of vortices led to a 53% increase in the surface- renewal rate, which increased the limiting (i.e., steady-state) permeate flux by 30%, decreased the specific cake resistance by 14.5% and decreased the limiting cake mass by 15.5% compared to operation without vortices. For the approximate model, a 50% increase in the value of surface renewal rate was shown to result due to vortices, which increased the limiting permeate flux by 30%, decreased the specific cake resistance by 10.5% and decreased the limiting cake mass by 13.7%. CFMF operation in the presence of Dean vortices reduced the total (limiting) mass of solids accumulated on the membrane surface by 6-7 mg. In the case of the complete model, the

RMS errors were 2.6 (no vortices) and 4.3% (with vortices), while those for the approximate model were 2.3 and 3.9%, respectively. One can speculate that, if more data were available at small values of the process time (see Figures 3 or 5), when the flux drops drastically, the complete model would have smaller errors than the approximate model.

The cake-filtration ($n$ = 0) version of the well-known critical-flux model of microfiltration (Field *et al*., 1995) was also compared against the experimental permeate-flux data of Mallubhotla and Belfort (1997). Although this model can represent these data, the quality of its fit is inferior compared to that of the surface-renewal model.

Dean vortices, by increasing flow instability, which is manifested in an increased rate of renewal of liquid elements at the membrane surface, can cause a looser, less compact cake, and a smaller buildup of cake on the membrane wall when compared to the situation when such vortices are absent. This allows for a heightened permeate flux with a quicker approach to steady-state, which is of paramount importance in CFMF. However, as discussed earlier, this effect is only manifested within a certain range of feed concentrations. The approximate two-parameter surface-renewal model mirrors its three-parameter counterpart and should be adequate for representing experimental permeate-flux data provided one starts the experiment with a clean membrane.

Overall, the surface-renewal model for CFMF was shown to be sensitive, consistent and precise since the RMS deviations of the model from experiment, as observed in this study, would most likely fall within the magnitude of the experimental error. The essence of the surface-renewal model is its ability to explicitly account for flow instabilities generated at the membrane surface (e.g., due to membrane roughness, presence of spacers, or vortices) through the hydrodynamic parameter $S$, in contrast to the other models of membrane filtration (e.g., the film, boundary-layer or resistance models). For future work, we suggest that the model be tested further by means of a rigorous experimental protocol for its ability to predict the influences of variables like transmembrane pressure drop, feed concentration and axial liquid velocity on the transient flux of permeate.

## ACKNOWLEDGEMENT

S. G. C. thanks Mr. Susumu Ikuta and Dr. Noshir Mistry for thought-provoking discussions on cross-flow microfiltration, which has had a significant influence on this work.

## NOMENCLATURE

| | |
|---|---|
| $A$ | filtration area (cm$^2$) |
| $c_b$ | mass of solids deposited in the filter per unit volume of filtrate (approximately equal to the concentration of solids in the feed or bulk liquid) (kg m$^{-3}$) |
| $d$ | half channel height [= $(R_2 - R_1)/2$] (mm) |
| $d_p$ | average nominal diameter of particles in the feed suspension (μm) |
| $D$ | Dean number ratio (= $De/De_c$) |
| $D_i$ | Diffusion coefficient of the dissolved gas in the liquid (m$^2$ s$^{-1}$) |
| $De$ | Dean number $[= (2du/\vartheta_s)\sqrt{2d/r_c}]$ |
| $De_c$ | Critical Dean number |
| $E$ | rate of cake erosion per unit area (kg m$^{-2}$ s$^{-1}$) |
| $E_{mod}$ | modified cake erosion parameter; defined by Eq. (28) (m s$^{-3}$) |
| $FE$ | Limiting or steady-state flux enhancement due to vortices; defined by Eq. (29) |
| $H$ | height of test cell (mm) |
| $J(t_p)$ | permeate flux at process time $t_p$ in the critical-flux model (m s$^{-1}$) |
| $J_a(t_p)$ | age-averaged permeate flux when the process time is $t_p$ (m s$^{-1}$) |
| $J_a^*(t_p^*)$ | dimensionless age-averaged permeate flux when the dimensionless process time is $t_p^*$; defined by Eq. (3) |
| $J_{crit}$ | critical permeate flux (m s$^{-1}$) |
| $J_{init}$ | permeate flux as $t_p \rightarrow 0$ (m s$^{-1}$) |
| $J_{init,1}$ | permeate flux as $t_p \rightarrow 0$ when no vortices are present (m s$^{-1}$) |
| $J_{init,2}$ | permeate flux as $t_p \rightarrow 0$ when vortices are present (m s$^{-1}$) |
| $J_{lim}$ | limiting or steady-state permeate flux (m s$^{-1}$) |
| $J_{lim,1}$ | limiting permeate flux when no vortices are present (m s$^{-1}$) |
| $J_{lim,2}$ | limiting permeate flux when vortices are present (m s$^{-1}$) |
| $J_{lim}^*$ | dimensionless limiting or steady-state permeate flux; $J_{lim}/J_0$ |
| $J_0$ | initial permeate flux (i.e., at $t_p$ = 0) (m s$^{-1}$) |
| $k$ | parameter in critical-flux model [s m$^{-2}$ ($n_c$ = 0), m$^{-1}$ ($n_c$ = 1), s$^{-1}$ ($n_c$ = 2)] |
| $K$ | constant in Eq. (31) |
| $k_c$ | defined by Eq. (7) (s m$^{-2}$) |
| $K_{cake}$ | cake-filtration constant in the critical-flux model (kg m$^{-3}$) |
| $k_L$ | mass-transfer coefficient (m s$^{-1}$) |
| $L$ | length of test cell (mm) |

$m_{c,a}(t_p)$ age-averaged cake mass per unit area of membrane surface at process time $t_p$ (kg m$^{-2}$)
$m^*_{c,a}(t^*_p)$ dimensionless age-averaged cake mass when the dimensionless process time is $t^*_p$; defined by Eq. (4)
$m_{c,init}$ mass of cake on the membrane surface as $t_p \to 0$ (kg m$^{-2}$)
$m_{c,init,1}$ mass of cake on the membrane surface as $t_p \to 0$ when no vortices are present (kg m$^{-2}$)
$m_{c,init,2}$ mass of cake on the membrane surface as $t_p \to 0$ when vortices are present (kg m$^{-2}$)
$m_{c,lim}$ limiting or steady-state cake mass (kg m$^{-2}$)
$m_{c,lim,1}$ limiting or steady-state cake mass when no vortices are present (kg m$^{-2}$)
$m_{c,lim,2}$ limiting or steady-state cake mass when vortices are present (kg m$^{-2}$)
$m^*_{c,lim}$ limiting or steady-state dimensionless cake mass (= $m_{c,lim}J_0k_c/c_b$)
$n$ compressibility coefficient of the cake
$n_c$ index in the critical-flux model; equals 0, 1, 1.5 or 2 depending upon the fouling mechanism
$n_1$ compressibility coefficient of the cake when no vortices are present
$n_2$ compressibility coefficient of the cake when vortices are present
$r_c$ centerline radius of the curved channel (mm)
$R_m$ hydraulic resistance of the membrane (m$^{-1}$)
$R_1$ radius of curvature of the inner wall of the curved channel (mm)
$R_2$ radius of curvature of the outer wall of the curved channel (mm)
$S$ rate of renewal of liquid elements at the membrane surface (s$^{-1}$)
$S_1$ surface-renewal rate when no vortices are present (s$^{-1}$)
$S_2$ surface-renewal rate when vortices are present (s$^{-1}$)
$S^*$ dimensionless surface-renewal rate; defined by Eq. (1)
$t_p$ process time (s)
$t^*_p$ dimensionless process time; defined by Eq. (2)
$u$ mean axial liquid or feed velocity (m/s or mm/s)
$W$ width of test cell (mm)
$x$ parameter of $\Gamma(x, y)$
$y$ parameter of $\Gamma(x, y)$

***Greek Symbols***

$\alpha$ specific cake resistance (m kg$^{-1}$)
$\alpha_1$ specific cake resistance when no vortices are present (m kg$^{-1}$)
$\alpha_2$ specific cake resistance when vortices are present (m kg$^{-1}$)
$\alpha_0$ constant in Eq. (20) (m kg$^{-1}$)
$\alpha_{01}$ value of $\alpha_0$ when no vortices are present (m kg$^{-1}$)
$\alpha_{02}$ value of $\alpha_0$ when vortices are present (m kg$^{-1}$)
$\Gamma(x, y)$ extended Euler gamma function; defined by Eq. (5)
$\delta$ arbitrarily small value of the process time (s)
$\Delta p$ transmembrane pressure drop (Pa or kPa)
$\varepsilon$ arbitrarily small value of the process time (s)
$\lambda$ variable of integration in Eq. (5)
$\mu$ viscosity of the permeate (kg m$^{-1}$ s$^{-1}$)
$\rho_p$ density of particles in the feed suspension (kg/m$^3$)
$\vartheta_s$ kinematic viscosity of the feed suspension (mm$^2$/s)
$\phi$ volume fraction of particles in the feed suspension
$\omega$ $S / \alpha_0$ (kg m$^{-1}$ s$^{-1}$)
$\omega_1$ $S_1 / \alpha_{01}$ (kg m$^{-1}$ s$^{-1}$)
$\omega_2$ $S_2 / \alpha_{02}$ (kg m$^{-1}$ s$^{-1}$)

## REFERENCES

Arnot, T. C., Field, R. W. and Koltuniewicz, A. B., Cross-flow and dead-end microfiltration of oily-water emulsions. Part II: Mechanisms and modeling of flux decline. J. Membrane Sci., 169, 1-15 (2000).

Bailey, S. M. and Meagher, M. M., The effect of denaturants on the crossflow membrane filtration of *Escherichia coli* lysates containing inclusion bodies. J. Membrane Sci., 131, 29-38 (1997).

Bailey, S. M. and Meagher, M. M., Crossflow microfiltration of recombinant *Escherichia coli* lysates after high pressure homogenization. Biotechnol. Bioeng., 56, 304-310 (1997).

Bailer-Jones, D. M., Scientific Models in Philosophy of Science. University of Pittsburgh Press, Pittsburgh, Pennsylvania (2009).

Chatterjee, S. G., On the use of the surface-renewal concept to describe cross-flow ultrafiltration. Indian Chemical Engineer, 52, 179-193 (2010).

Cheryan, M., Ultrafiltration Handbook. Technomic Publishing Company, Inc., Lancaster, Pennsylvania (1986).

Cheryan, M., Ultrafiltration and Microfiltration Handbook. Second Ed., CRC Press, Boca Raton, Florida (1998).

Chung, K. Y., Brewster, M. E. and Belfort, G., Dean vortices with wall flux in a curved channel membrane system: 2. The velocity field. AIChE J., 42, 347-358 (1996).

Chung, K. Y., Brewster, M. E. and Belfort, G., Dean vortices with wall flux in a curved channel membrane system: 3. Concentration polarization in a spiral reverse osmosis slit. J. Chem. Eng., Japan, 31, 683-693 (1998).

Constenla, D. T. and Lozano, J. E., Predicting stationary permeate flux in the ultrafiltration of apple juice. Lebensm. Wiss. u. Technol., 29, 587-592 (1996).

Danckwerts, P. V., Significance of liquid-film coefficients in gas absorption. Ind. Eng. Chem. (Eng. and Process Dev.), 43, 1460-1467 (1951).

Danckwerts, P. V., Gas–Liquid Reactions. McGraw-Hill, New York (1970).

Field, R. W., Wu, D., Howell, J. A. and Gupta, B. B., Critical flux concept for microfiltration fouling. J. Membrane Sci., 100, 259-272 (1995).

Gehlert, G., Luque, S. and Belfort, G., Comparison of ultra- and microfiltration in the presence and absence of secondary flow with polysaccharides, proteins, and yeast suspensions. Biotechnol. Prog., 14, 931-942 (1998).

Gurian, P. L., Microfiltration cost benchmarking for large facilities. iDEA: Drexel E-repository and Archives, Faculty Research and Publications (CAEE), http://hdl.handle.net/1860/3168 (2010).

Hasan, A., Yasarla, R., Ramarao, B. V. and Amidon, T. E., Separation of lignocellulosic hydrolyzate components using ceramic microfilters. J. Wood Chem. Technol., 31, 357-383 (2011).

Hasan, A., Peluso, C. R., Hull, T. S., Fieschko, J. and Chatterjee, S. G., A surface-renewal model of cross-flow microfiltration. Brazilian Journal of Chemical Engineering, 30, 167-186 (2013).

Huang, L. and Morrissey, M. T., Fouling of membranes during microfiltration of Surimi wash water: Roles of pore blocking and surface cake formation. J. Membrane Sci., 144, 113-123 (1998).

Hutchinson, M. H. and Sherwood, T. K., Liquid film in gas absorption. Ind. Eng. Chem., 29, 836-840 (1937).

Koltuniewicz, A., Predicting permeate flux in ultrafiltration on the basis of surface renewal concept. J. Membrane Sci., 68, 107-118 (1992).

Koltuniewicz, A. and Noworyta, A., Dynamic properties of ultrafiltration systems in light of the surface renewal theory. Ind. Eng. Chem. Res., 33, 1771-1779 (1994).

Koltuniewicz, A. and Noworyta, A., Method of yield evaluation for pressure-driven membrane processes. Chem. Eng. J., 58, 175-182 (1995).

Kovalsky, P., Bushell, G. and Waite, T. D., Prediction of transmembrane pressure build-up in constant flux microfiltration of compressible materials in the absence and presence of shear. J. Membrane Sci., 344, 204-210 (2009).

Kroner, K. H., Schutte, H., Hustedt, H. and Kula, M., Cross-flow filtration in the downstream processing of enzymes. Process Biochem., 19, 67-74 (1984).

Le, M. S., Spark, L. B., Ward, P. S. and Ladwa, N., Microbial asparaginase recovery by membrane processes. J. Membrane Sci., 21, 307-319 (1984).

Luque, S., Mallubhotla, H., Gehlert, G., Kuriyel, R., Dzengeleski, S., Pearl, S. and Belfort, G., A new coiled hollow-fiber module design for enhanced microfiltration performance in biotechnology. Biotech. Bioeng., 65, 247-257 (1999).

Mallubhotla, H. and Belfort, G., Flux enhancement during Dean vortex microfiltration. 8. Further diagnostics. J. Membrane Sci., 125, 75-91 (1997).

Mallubhotla, H., Hoffmann, S., Schmidt, M., Vente, J. and Belfort, G., Flux enhancement during Dean vortex tubular membrane nanofiltration. 10. Design, construction, and system characterization. J. Membrane Sci., 141, 183-195 (1998).

Mallubhotla, H., Schmidt, M., Lee, K. H. and Belfort, G., Flux enhancement during Dean vortex tubular membrane nanofiltration. 13. Effects of concentration and solute type. J. Membrane Sci., 153, 259-269 (1999).

Mallubhotla, H., Belfort, G., Edelstein, W. A. and Early, T. A., Dean vortex stability using magnetic resonance flow imaging and numerical analysis. AIChE J., 47, 1126-1140 (2001).

Marston, F. A. O., Lowe, P. A., Doel, M. T., Schoemaker, S., White, S. and Angal, S., Purification of calf prochymosin (prorennin) synthesized in *Escherichia coli*. Nature Biotechnology, 2, 800-804 (1984).

McCabe, W. L., Smith, J. C. and Harriott, P., Unit Operations of Chemical Engineering. Fifth Ed., McGraw-Hill, New York (1993).

Perry, R. H., Green, D. W. and Maloney, J. O., Eds., Perry's Chemical Engineers' Handbook. Sixth Ed., McGraw-Hill, New York (1984).

Richardson, J. F., Harker, J. H. and Backhurst, J. R., Coulson and Richardson's Chemical Engineering.

Vol. 2, Fifth Ed., Butterworth-Heinemann, Oxford, UK (2002).

Rudolph, E. A. and MacDonald, J. H., Tangential Flow Filtration Systems for Clarification and Concentration. In: Bioprocess Engineering: Systems, Equipment and Facilities, Lydersen, B. K., D'Elia, N. A. and Nelson, K. L., Eds., p. 119-157, John Wiley & Sons, Inc., New York (1994).

Sarkar, D., Datta, D., Sen, D. and Bhattacharjee, C., Simulation of continuous stirred rotating disk-membrane module: An approach based on surface renewal theory. Chem. Eng. Sci., 66, 2554-2567 (2011).

Shoner, R. G., Ellis, L. F. and Shoner, B. E., The isolation and purification of protein granules from *Escherichia coli* cells overproducing bovine growth hormone. Nature Biotechnology, 3, 151-154 (1985).

Song, L., Flux decline in crossflow microfiltration and ultrafiltration: Mechanisms and modeling of membrane fouling. J. Membrane Sci., 139, 183-200 (1998).

Titchener-Hooker, N. J., Gritisis, D., Mannweiler, K., Olbrich, R., Gardiner, S. A. M., Fish, N. M. and Hoare, M., Integrated process design for producing and recovering proteins from inclusion bodies. BioPharm, 4, 34-38 (1991).

Zhang, W. and Chatterjee, S. G., Influence of residence time distribution on a surface-renewal model of constant-pressure, cross-flow microfiltration. Brazilian Journal of Chemical Engineering, 32(1), 139-154 (2015).

## APPENDIX

In this section, we present a qualitative analysis of the behavior of the permeate flux and cake buildup on the membrane surface as a function of process time with the aid of the approximate model. Let $\delta$ and $\varepsilon$ be two arbitrarily small values (close to zero) of the process time $t_p$ with $\delta < \varepsilon$. We designate the time periods of $0 < t_p < \delta$ and $\delta < t_p < \varepsilon$ as the initial moments and initial period of filtration, respectively. It is assumed that, during the initial moments of filtration (where the permeate flux drops drastically), a cake layer is formed that completely covers the membrane surface. The specific resistance $\alpha$ of the cake is assumed to remain invariant with the subsequent passage of time, i.e., for $t_p > \delta$. Let $J_{init}$ and $m_{c,init}$ be the permeate flux and mass of cake, respectively, at a specific value of $t_p$ which lies in the range $\delta < t_p < \varepsilon$. Using subscripts 1 and 2 to denote the situations without and with vortices, respectively, and assuming $\Delta p$, $\mu$ and $c_b$ to be the same with and without vortices, Eqs. (16) – (19) give:

$$\frac{J_{init,2}}{J_{init,1}} = \frac{m_{c,init,2}}{m_{c,init,1}} = \sqrt{\frac{\alpha_1}{\alpha_2}} \tag{A1}$$

$$\frac{J_{lim,2}}{J_{lim,1}} = \sqrt{\frac{S_2}{S_1}}\sqrt{\frac{\alpha_1}{\alpha_2}} \tag{A2}$$

$$\frac{m_{c,lim,2}}{m_{c,lim,1}} = \sqrt{\frac{S_1}{S_2}}\sqrt{\frac{\alpha_1}{\alpha_2}} \tag{A3}$$

It should be noted that $S_2 > S_1$. The following three cases are possible:

**Case 1: $\alpha_1 > \alpha_2$**

In this case, Eqs. (A1) and (A2) imply that $J_{init,2} > J_{init,1}$, $m_{c,init,2} > m_{c,init,1}$ and $J_{lim,2} > J_{lim,1}$. The permeate-flux behavior is sketched in Figure A1(a) where it is seen that the permeate flux with vortices is greater compared to that without vortices. The following three subcases are possible for the behavior of the cake mass:

(i) If $\alpha_1 / \alpha_2 > S_2 / S_1$, $m_{c,lim,2} > m_{c,lim,1}$ [Eq. (A3)]. The cake-mass curve with vortices lies above that without vortices [Figure A1[b(i)] because of the greater accumulation of solids on the membrane surface due to the larger permeate flux in the presence of vortices.

(ii) If $\alpha_1 / \alpha_2 < S_2 / S_1$, $m_{c,lim,2} < m_{c,lim,1}$ [Eq. (A3)]. Figure A1[b(ii)] shows that the cake-mass with vortices is initially greater compared to that without vortices, but at a certain value of the process time, the curves cross each other, after which the cake accumulation with vortices is smaller than that without vortices. Figures A1(a) and A1[b(ii)] represent the base case of the experimental data of Mallubhotla and Belfort (1997), which was discussed earlier.

(iii) If $\alpha_1 / \alpha_2 = S_2 / S_1$, $m_{c,lim,2} = m_{c,lim,1}$ [Eq. (A3)]. The cake-mass curve in the presence of vortices lies above the cake-mass curve when they are absent and, as the process time increases, both curves converge to the same limiting value [Figure A1[b(iii)].

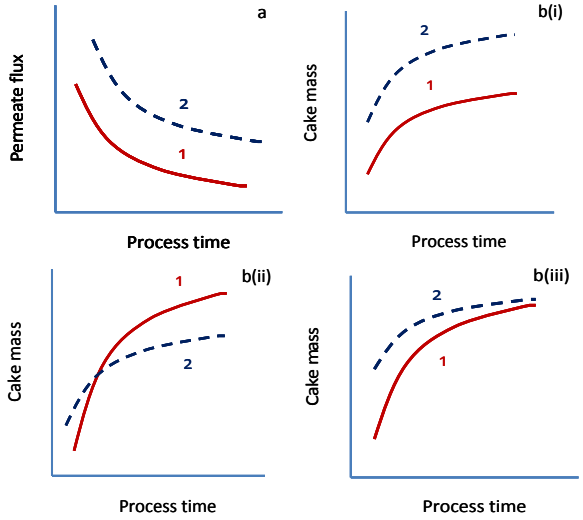


**Figure A1:** Behavior of permeate flux and cake accumulation on the membrane surface as a function of process time for $\alpha_1 > \alpha_2$ (Case 1). Figure b(i): $\alpha_1 / \alpha_2 > S_2 / S_1$ ; Figure b(ii): $\alpha_1 / \alpha_2 < S_2 / S_1$ and Figure b(iii): $\alpha_1 / \alpha_2 = S_2 / S_1$. 1≡ without vortices; 2 ≡ with vortices.

### Case 2: $\alpha_1 = \alpha_2$

It follows from Eqs. (A1) – (A3) that $J_{init,2} = J_{init,1}$, $m_{c,init,2} = m_{c,init,1}$, $J_{lim,2} > J_{lim,1}$, and $m_{c,lim,2} < m_{c,lim,1}$ Figures A2(a) and A2(b) show that the permeate-flux and cake-mass curves with and without vortices are convergent at small values of the process time, whereas they diverge away from one another as the process time increases. Vortices cause a greater permeate flux and smaller cake accumulation on the membrane surface.

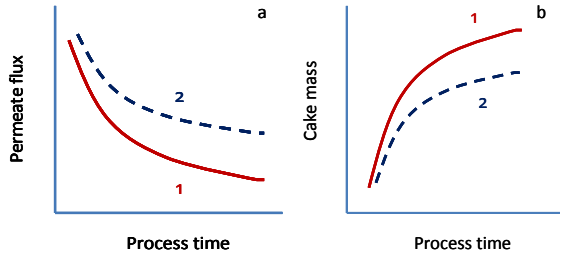


**Figure A2:** Behavior of permeate flux and cake accumulation on the membrane surface as a function of process time for $\alpha_1 = \alpha_2$ (Case 2). 1≡ without vortices; 2 ≡ with vortices.

### Case 3: $\alpha_1 < \alpha_2$

From Eqs. (A1) and (A3) it can be deduced that $J_{init,2} < J_{init,1}$, $m_{c,init,2} < m_{c,init,1}$ and $m_{c,lim,2} < m_{c,lim,1}$. The behavior of cake accumulation on the membrane wall is shown in Figure A3(a), where it is observed that vortices lead to a lower cake accumulation. The following three subcases are possible for the behavior of the permeate flux:

(i) If $\alpha_2 / \alpha_2 < S_2 / S_1$, $J_{lim,2} > J_{lim,1}$ [Eq. (A2)]. The permeate flux without vortices is higher than that with vortices up to a certain value of the process time, beyond which they cross one another [Figure A3[b(i)].

(ii) If $\alpha_2 / \alpha_2 > S_2 / S_1$, $J_{lim,2} < J_{lim,1}$ [Eq. (A2)]. Permeate flux in the absence of vortices is larger than when they are present [Figure A3[b(ii)], i.e., vortices have a negative effect.

(iii) If $\alpha_2 / \alpha_2 = S_2 / S_1$, $J_{lim,2} = J_{lim,1}$ [Eq. (A2)]. Vortices cause a lower permeate flux compared to that when they are absent, with the difference between them gradually diminishing as the steady-state is approached [Figure A3[b(iii)].

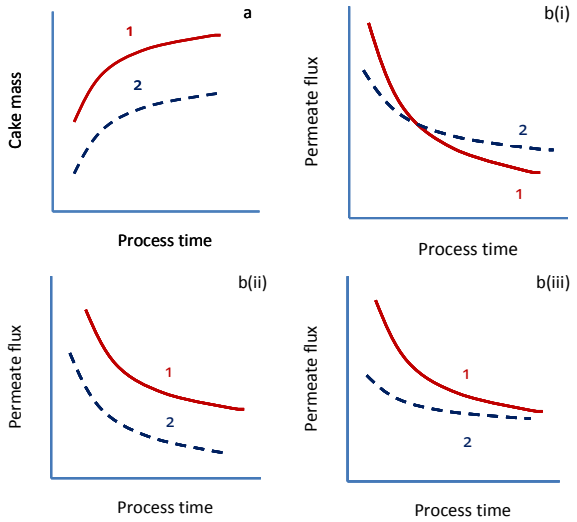


**Figure A3:** Behavior of cake accumulation on the membrane surface and permeate flux as a function of process time for $\alpha_1 < \alpha_2$ (Case 3). Figure b(i): $\alpha_2 / \alpha_2 < S_2 / S_1$ ; Figure b(ii): $\alpha_2 / \alpha_2 > S_2 / S_1$ and Figure b(iii): $\alpha_2 / \alpha_2 = S_2 / S_1$. 1≡ without vortices; 2 ≡ with vortices.